The University of Sydney

School of Civil Engineering
Sydney NSW 2006
AUSTRALIA

http://www.civil.usyd.edu.au/

Centre for Advanced Structural Engineering

Finite Element Analysis of Structural Steel Elliptical Hollow Sections in Compression

Research Report No R874

Yi Zhu BE
Tim Wilkinson BSc BE MA PhD

February 2007

The University of Sydney

School of Civil Engineering
Centre for Advanced Structural Engineering
http://www.civil.usyd.edu.au/

Finite Element Analysis of Structural Steel Elliptical Hollow Sections in Compression

Yi Zhu, BE
Tim Wilkinson, BSc, BE, MA, PhD

Abstract:

This paper presents a finite element investigation of the local buckling behaviour of the structural steel Elliptical Hollow Section (EHS) in compression. The theoretical elastic buckling load of an EHS is similar to that of a Circular Hollow Section (CHS) except that the diameter term, D, is replaced by D_1^2/D_2, representing the major and minor diameters of the ellipse. The overall aim is to examine whether an "equivalent CHS" can be used to model the local buckling of EHS when considering imperfections and non-linear material properties. The finite element program ABAQUS was used to examine the local buckling behaviour of EHS with a range of aspect ratios from 1:1 (CHS) to 10:1 to examine the transitional behaviour. Three types of analysis were considered. The first stage was elastic buckling with no material imperfection. The second stage considered inelastic material properties, followed by measured material properties. The final stage was to investigate how geometric imperfection affected the buckling modes. The results are benchmarked against experimental results. It was found that the use of an equivalent CHS was a reasonably good predictor of capacity of slender sections and the deformation capacity of compact sections. However, further benchmarking against experimental results is recommended.

Keywords:

Elliptical Hollow Section; Local buckling; Finite element analysis; ABAQUS

Copyright Notice

School of Civil Engineering, Research Report R874
Finite Element Analysis of Structural Steel Elliptical Hollow Sections in Compression
© 2007 Yi Zhu & Tim Wilkinson
y.zhu@civil.usyd.edu.au
wilko@civil.usyd.edu.au

ISSN 1833-2781

CONTENTS

1 Background

The Elliptical Hollow Section (EHS) is a relatively new shape of high strength, hot-rolled steel sections. It is being used in structural building applications due to its unique aesthetics. Elliptical sections also offer the structural advantages of sections with differing major and minor axis properties, compared with circular hollow sections.

Broad application of EHS requires fundamental and systematical test data to verify structural design guidance of EHS. However, despite interest in their usage, currently test results are insufficient and there is a limited understanding of properties and structural performance of elliptical sections.

Past research has been performed on Circular Hollow Section regarding the local buckling behaviour. Equation 1 gives the expression to calculate the elastic buckling stress of a CHS subject to pure compression.

$$\sigma_{cr} = \frac{2Et}{D\sqrt{3(1-v^2)}} \ \dots\dots\dots\dots\dots\dots\dots\dots\dots\dots\dots\dots\dots\dots\dots\dots\dots\dots \ (1)$$

where E is the material Young's modulus, t is the thickness of the circular cross section, v is Poisson's ratio and D is the diameter. From this equation, it can be seen that the ratio of D/t is the key parameter affecting local buckling of CHS.

In the 1950s and 1960s, the elastic critical buckling and post-buckling behaviour of elliptical shells first received attention in the USA. From these initial studies, formulae to predict the elastic critical buckling and post-buckling response of elliptical hollow sections under axial loading were derived (Marguerre, 1951 and Kempner, 1962). The elastic critical buckling stress for an elliptical cross section (whose geometry is defined by the equation of an ellipse) subjected to pure compression is given by Equation 2.

$$\sigma_{cr} = \frac{Et}{\left(\dfrac{A^2}{B}\right)\sqrt{3(1-v^2)}} \ \dots\dots\dots\dots\dots\dots\dots\dots\dots\dots\dots\dots\dots\dots\dots\dots\dots\dots \ (2)$$

where A and B are the major and minor radii, respectively, as shown in Figure 1.
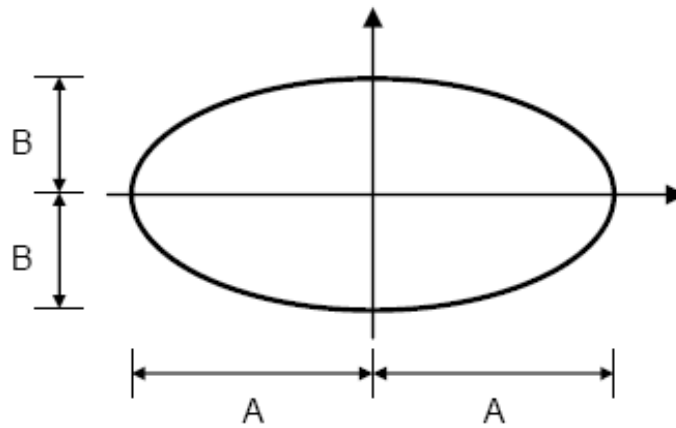
Figure 1. Geometry of Elliptical Sections

The form of Equation 2 is very similar to that of Equation 1. By changing both formulas slightly and replace $2A$ and $2B$ as D_1 and D_2 which refer to the length of major and minor diameter of an ellipse respectively, it can be concluded that an EHS can be considered equivalent to a CHS whose diameter is $D = \dfrac{D_1^2}{D_2}$. Indeed for the case where A equals B, Equation 2 reverts exactly to Equation 1.

Currently, hot-finished Elliptical Hollow Sections are supplied in accordance with the Euronorm EN 10210. The sizes of available products in UK market are in the range of $D_1/t = 15 - 80$, $D_1/D_2 = 2$.

Recent work by Gardner, L. (2005) introduced a series of compression tests and bending tests on elliptical hollow sections, followed by numerical modeling. In this study, the models included features such as curved geometry, non-linear material properties and initial geometric imperfections. The test and finite element results were compared with preliminary rules for section classification of elliptical hollow sections. Although the classification limits were shown to be broadly acceptable, further test and finite element results for a thorough validation were required.

This paper will further investigate the relationship between EHS and CHS through finite element analysis, benchmarked against unpublished test results from The University of Toronto (2005).

2 Finite Element Analysis

2.1 Element type

Finite element analyses were performed using ABAQUS to simulate the local buckling behaviour of the stub columns of EHS and CHS. ABAQUS includes general-purpose shell elements as well as elements that are valid for thick and

thin shell problems. The element type S4R was used in this study. S4R is a general-purpose, finite-membrane-strain, reduced integration shell element. The ratio of the length to width of the element is about 1:1. For the whole column, different mesh densities were adopted. In the transverse direction, a higher mesh density was used in the tighter corners of the higher aspect ratio ellipses. In the longitudinal direction, the mesh density was kept consistence. Typically a model had elements around the circumference and elements along the length. The mesh density for ABAQUS models of EHS and CHS sections is shown in Figure 2(a) and (b).
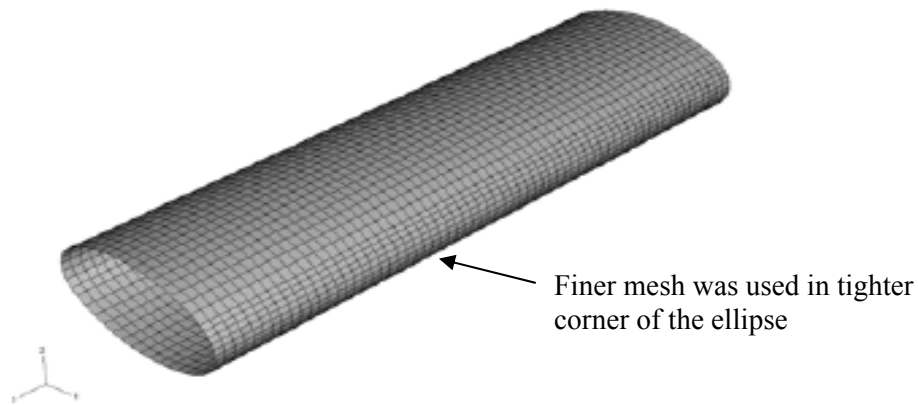
Figure 2(a). ABAQUS Mesh of EHS Columns
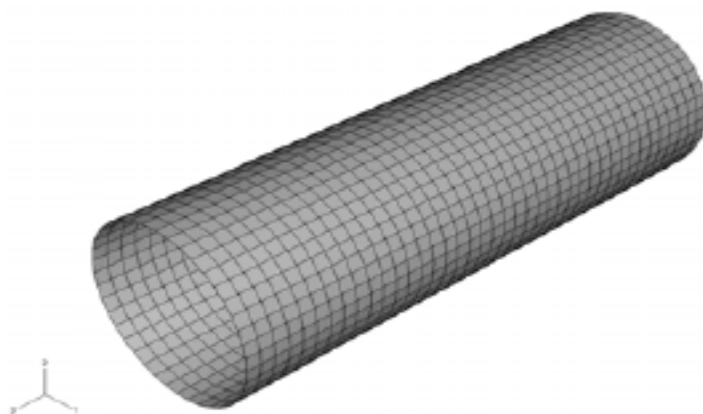
Figure 2(b). ABAQUS Mesh of CHS Columns

2.2 Material behaviour

Most materials of engineering interest initially respond elastically. If the load exceeds some limit, some part of the deformation will remain when the load is removed. Plasticity theories model the mechanical response of the material as it undergoes such nonrecoverable deformation in a ductile fashion. Most of the plasticity models in ABAQUS are "incremental" theories in which the mechanical strain rate is decomposed into an elastic part and a plastic part.

This project considered different material properties in different analysis stages as detailed in the following chapters.

2.3 Boundary conditions

For each of the two ends, two different types of boundary conditions were used to simulate the test situation in the column tests. The ends were divided into a fixed end and a movable end. At the fixed end, displacement degrees of freedom in 1, 2, 3 directions (U_1, U_2, U_3) as well as rotational degrees of freedom in 1, 2, 3 directions (θ_1, θ_2, θ_3) were restrained to be zero. At the movable end, load was exerted with an even stress distribution in the longitudinal direction U_3. The simplified representation of boundary conditions is shown in Figure 3.
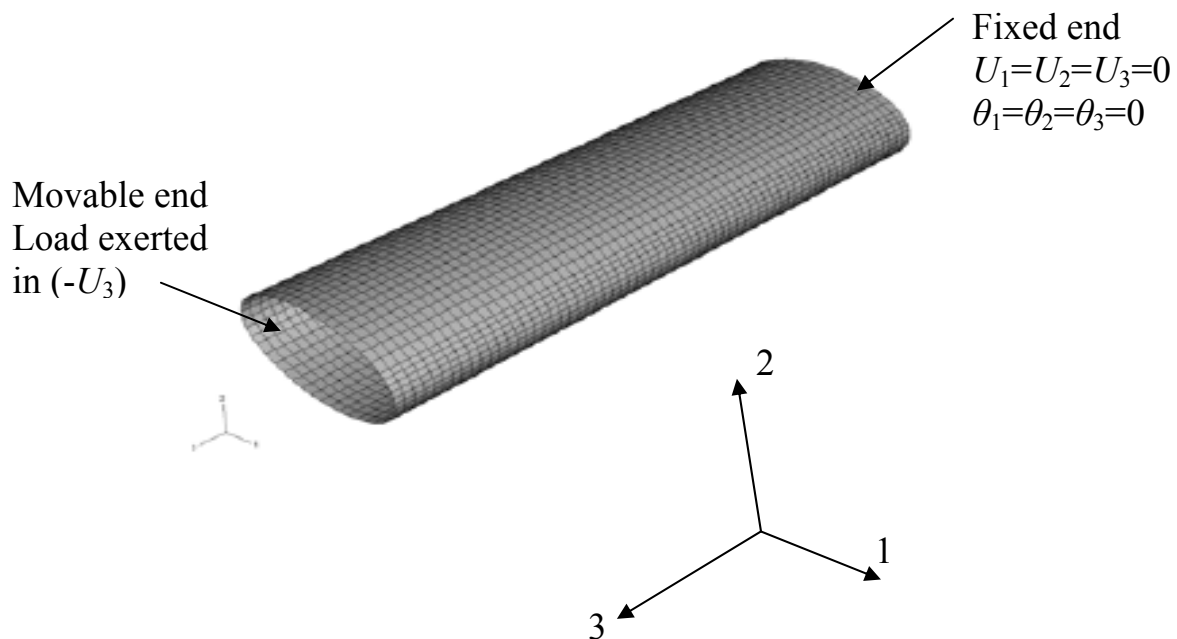
Figure 3. Boundary conditions for EHS in compression

2.4 Geometric imperfection

For ABAQUS, the approach to define an imperfection in this paper involved two analysis runs with the same model definition: (a) In the first analysis run, an eigenvalue buckling analysis was performed on the "perfect" structure to establish probable collapse modes and to verify that the mesh discretises those modes accurately. (b) In the second analysis run, an imperfection in the geometry was introduced by adding these buckling modes to the "perfect" geometry. (c) Finally, a geometrically nonlinear load displacement analysis of the structure was performed containing the imperfection using the Riks method. In this way the Riks method could be used to perform post-buckling analyses of "stiff" structures that show linear behaviour prior to buckling, if perfect. By performing a load-displacement analysis, other important nonlinear effects, such as material inelasticity or contact, can be included.

3 FEA Procedures of EHS and CHS Columns

3.1 Pure elastic buckling

The first stage was pure elastic buckling. The analysis was performed on EHS with a range of aspect ratios of major and minor axis from 1:1 (CHS) to 3:1 to examine the transitional behaviour.

3.1.1 FEA model
Nominally a CHS with diameter of 400 mm and length of 1200 mm was chosen for analysis. Various degrees of aspect ratio of the ellipse (D_1:D_2) were used: D_1/D_2 = 1.00, 1.25, 1.50, 1.75, 2.00, 2.25, 2.50, 2.75, and 3.00. Meanwhile, different slenderness values were achieved with D/t ranging from 20 to 120 by varying t. Thus, 9 different groups with 21 different models in each group were set up. Totally 189 models were simulated using ABAQUS.

The material properties of the models were assumed as pure elastic, which means no plastic data other than $E = 200 \times 10^9 \, \mathrm{Pa}, \nu = 0.3$ as elastic data were input.

3.1.2 Analysis method
Eigenvalue buckling analysis was generally used to estimate the critical bucking loads of stiff structures. An incremental loading pattern was defined in *BUCKLE step. A general eigenvalue buckling analysis can provide useful estimates of collapse mode shapes and calculate the buckling stress as well. The equation for calculation of buckling stress can be written as Equation 3.

$$\sigma_{cr} = E \cdot \varepsilon = E \cdot \lambda \cdot \frac{\Delta l}{l} \dots\dots\dots\dots\dots\dots\dots\dots\dots\dots\dots\dots\dots\dots\dots\dots\dots\dots\dots\dots (3)$$

where E is the material Young's modulus, λ is the eigenvalue obtained from the results of FEA, Δl is the initial displacement at the movable end input in the boundary conditions in ABAQUS, l is the length of the column.

3.1.3 Results

The nine groups of EHS column models were simulated using ABAQUS. With the results of eigenvalues obtained, the buckling stress of each model was calculated. On the other hand, knowing the geometry of each model, the buckling stress can be calculated from Equation 2. The summarized results showing the comparison between ABAQUS simulation and Equation 2 were demonstrated in Table 1 and Figure 4. A typical group of results for models with same aspect ratio (D_1/D_2 = 2.00) but different slenderness (various thicknesses) was shown in Table 2. All the other relative results were listed in Tables 11 to 19 in the Appendix.

D_1/D_2	$f_{ol,equation2} \big/ f_{ol,ABAQUS}$	
	Mean value	Standard deviation
1.00	1.01	0.04
1.25	0.94	0.01
1.50	0.92	0.01
1.75	0.91	0.02
2.00	0.90	0.02
2.25	0.89	0.02
2.50	0.89	0.02
2.75	0.88	0.02
3.00	0.88	0.02

Table 1. Difference between ABAQUS Results and Calculated Results from Equation 2

| $D_1/D_2 = 2.00$ | | | | | |
| Section Properties | | | Buckling Stress from ABAQUS (GPa) | Buckling Stress from Equation 2 (GPa) | Difference |
D_1 (mm)	D_2 (mm)	D_1/t			
400	200	20	7.05	6.04	14.33%
400	200	25	5.65	4.83	14.37%
400	200	30	4.68	4.03	13.83%
400	200	35	3.97	3.46	12.96%
400	200	40	3.45	3.02	12.21%
400	200	45	3.04	2.69	11.67%
400	200	50	2.72	2.42	11.17%
400	200	55	2.46	2.20	10.73%
400	200	60	2.25	2.02	10.43%
400	200	65	2.07	1.86	10.01%
400	200	70	1.91	1.73	9.71%
400	200	75	1.78	1.61	9.48%
400	200	80	1.67	1.51	9.31%
400	200	85	1.57	1.42	9.21%
400	200	90	1.48	1.34	8.85%
400	200	95	1.40	1.27	8.77%
400	200	100	1.32	1.21	8.65%
400	200	105	1.26	1.15	8.52%
400	200	110	1.20	1.10	8.49%
400	200	115	1.15	1.05	8.33%
400	200	120	1.10	1.01	8.08%

Table 2. Elastic Buckling Stress from ABAQUS Results and Equation 2 Results
for Model $D_1/D_2 = 2.00$
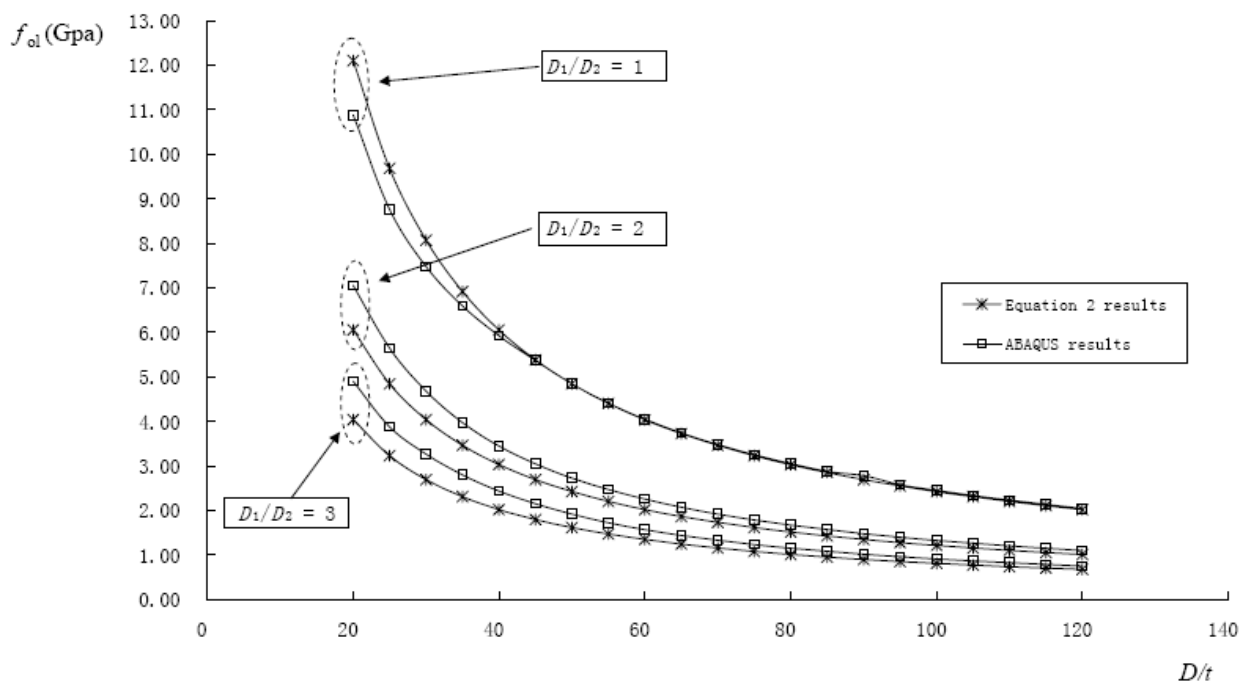
Figure 4. Some Results of Elastic Buckling Stress from ABAQUS and
Equation 2

The initial buckling shapes of EHS ($D_1/D_2 = 2.00$, $D_1/t = 30$) were shown in Figure 5. The maximum outward deformation of its cross section when buckling was observed as shown in Figure 6. The deformation of the middle cross section was shown in Figure 7.
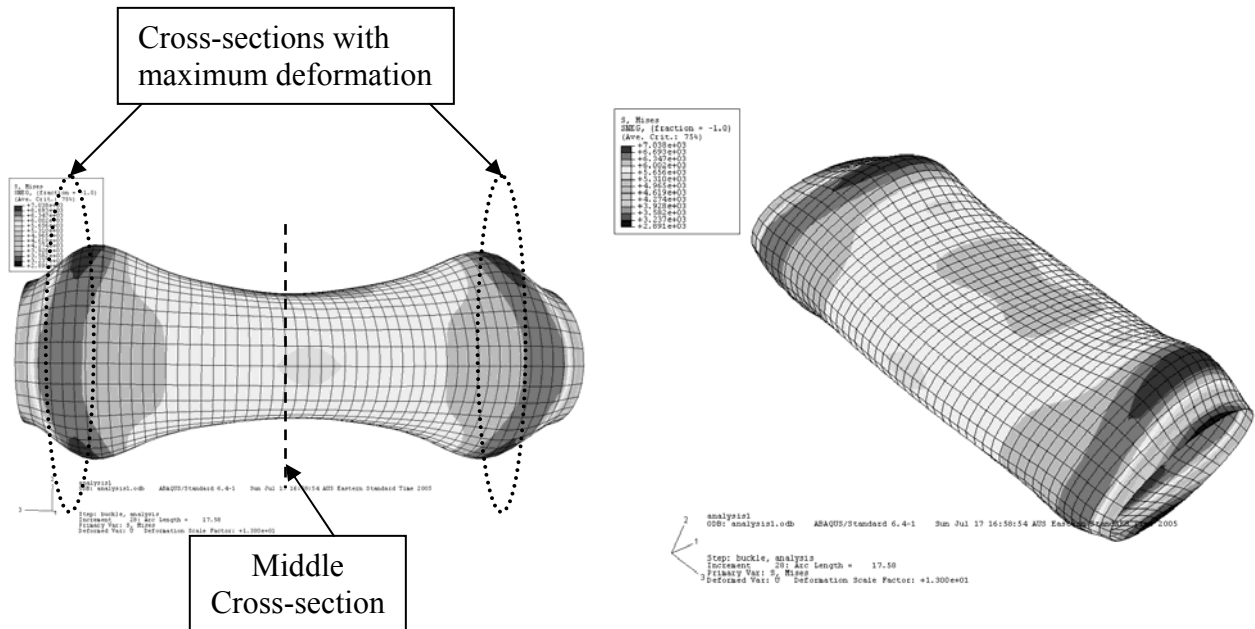
Figure 5. Initial Buckling Shapes of EHS ($D_1/D_2 = 2.00$, $D_1/t = 30$)
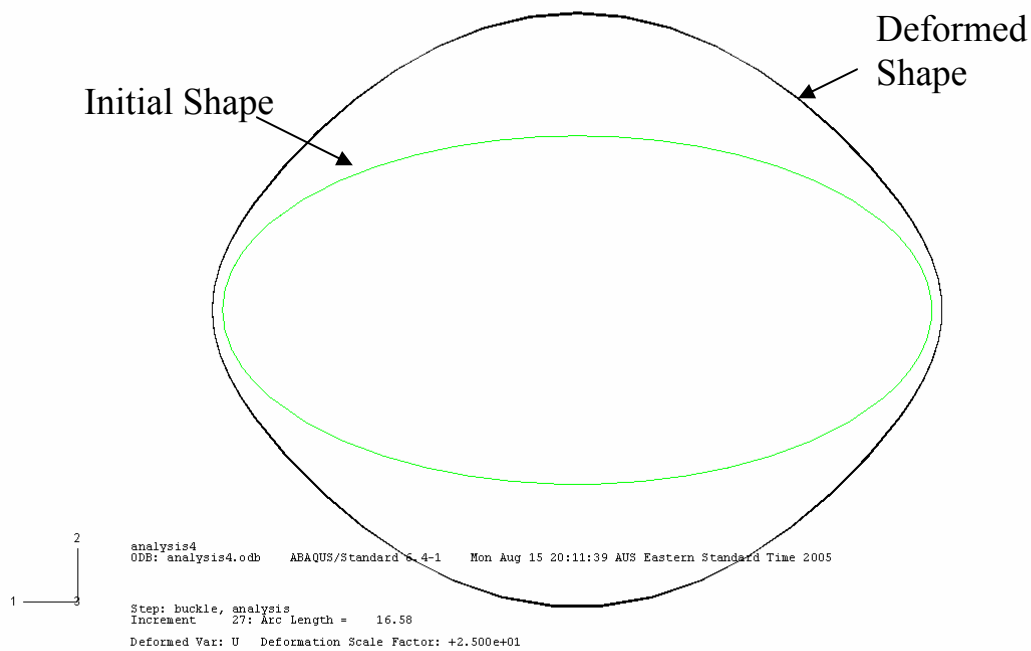
Figure 6. The Maximum Outward Deformation of the Cross Section
(EHS: $D_1/D_2 = 2.00$, $D_1/t = 30$)

```
2
|
1 ___|___ 3

analysis4
ODB: analysis4.odb    ABAQUS/Standard 6.4-1    Mon Aug 15 20:11:39 AUS Eastern Standard Time 2005

Step: buckle, analysis
Increment    27: Arc Length =    16.58
Deformed Var: U   Deformation Scale Factor: +3.000e+01
```
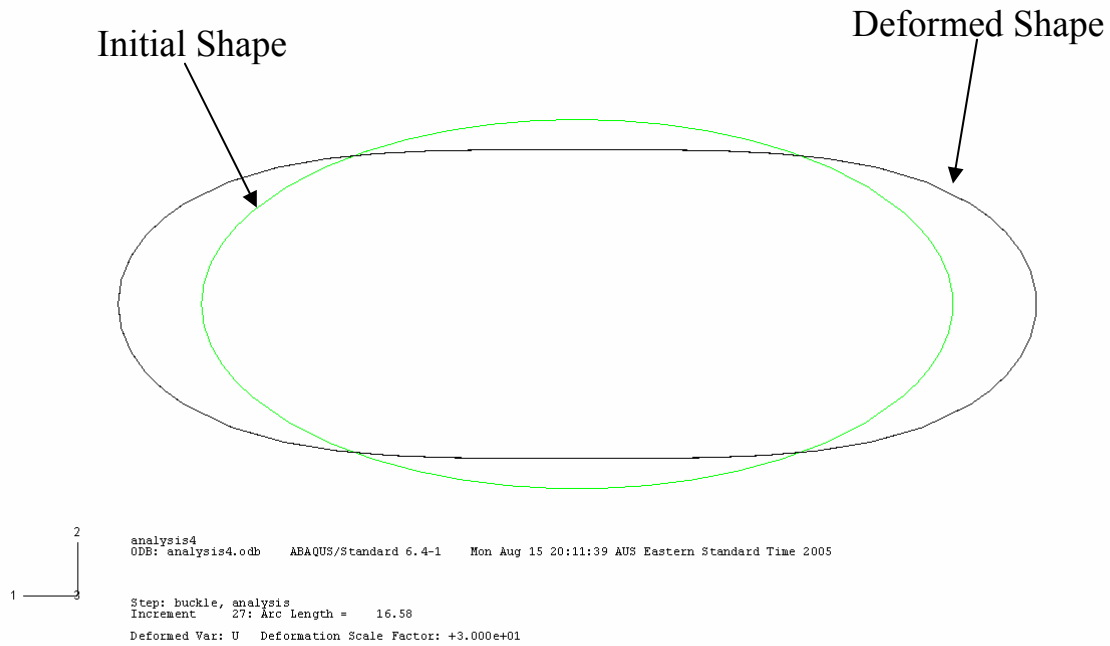
Figure 7. The Deformation of the middle cross-section
(EHS: $D_1/D_2 = 2.00$, $D_1/t = 30$)

Figure 8 shows the maximum outward deformation of its cross section when buckling for an EHS ($D_1/D_2 = 3.00$, $D_1/t = 30$).


```
2
|
1 ___|___ 3

analysis4
ODB: analysis4.odb    ABAQUS/Standard 6.4-1    Sat Aug 06 15:49:23 AUS Eastern Standard Time 2005

Step: buckle, analysis
Increment    18: Arc Length =    7.585
Deformed Var: U   Deformation Scale Factor: +1.000e+01
```
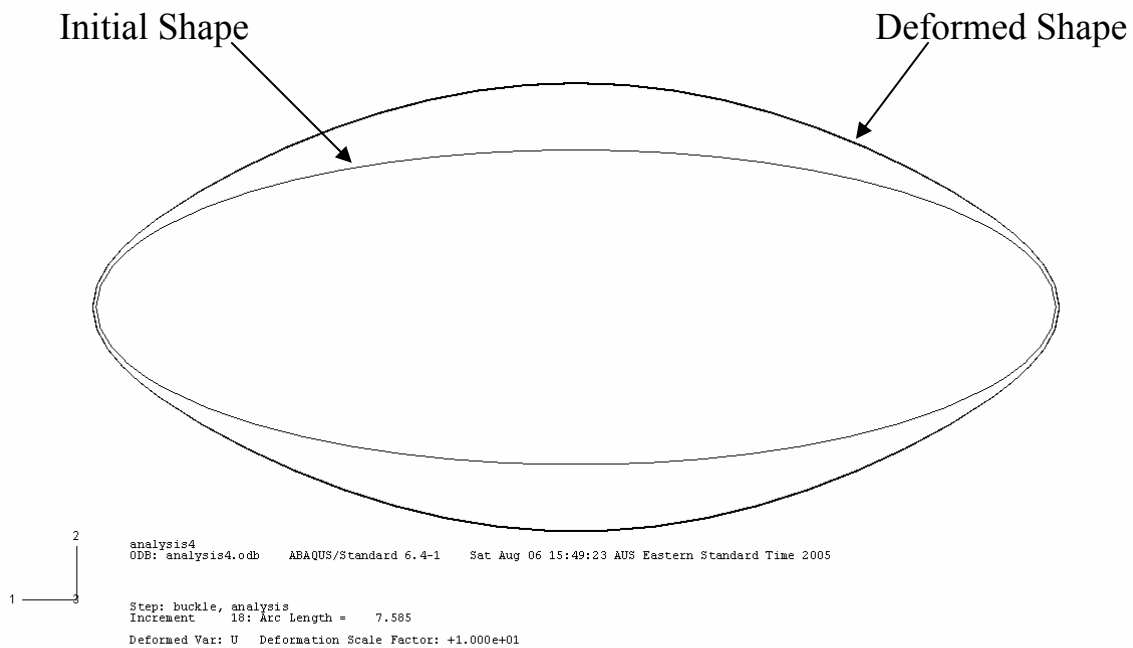
Figure 8. The Maximum Outward Deformation of the Cross Section
(EHS: $D_1/D_2 = 3.00$, $D_1/t = 30$)

3.1.4 Discussion

The elastic buckling stresses obtained from ABAQUS as well as Equation 2 were compared with each other. The results illustrate that the discrepancy between numerical and theoretical elastic buckling stresses for EHS is similar that of CHS. However, the difference was significantly influenced by the change of geometric properties of EHS as explained below.

Table 1 shows that for CHS (D_1:D_2 = 1.00), ABAQUS results and Equation 2 results match closely, within 1%, whereas for moderate aspect ratios such as D_1:D_2 = 1.50, the mean value of difference is approximately 5%, which is in a close range. However, for higher aspect ratios (D_1:D_2 > 1.50), the elastic buckling stress calculated from Equation 2 is consistently about 10% less than that from ABAQUS.

Table 2 demonstrates that for the same aspect ratio (D_1/D_2 = 2.00), the difference between ABAQUS results and Equation 2 results increases from 8% to 14% with the changing of D_1/t ratio from 120 to 20. This indicates that the discrepancy is also be affected by the slenderness values of an ellipse, which is also reflected in Figure 4.

Figure 6 shows that the local buckling shape for an EHS (D_1/D_2 = 2.00) involves outward deformation of all points on the cross-section, similar to the "elephant foot" buckling of a CHS. It is noted that near the area of lower radius of curvature (sharp corners) of the EHS, the outward deformation is less than that at the area of higher radius of curvature (wider faces). This finding matches the observation the experiments from Gardner, L. (2005). This can be explained by saying that the areas of higher radius of curvature of the ellipse are stiffer, and hence the deformation is less. Figure 8 shows the maximum outward deformation of another EHS (D_1/D_2 = 3.00, D_1/t = 30). It is observed that all EHS, regardless of aspect ratio, experience similar buckling shapes described above.

Figure 7 shows the deformation of the middle cross-section of an EHS. The near the sharp corners, the deformation goes outwards, while the wider faces goes inwards. This type of deformation shape (or buckling shape) is also consistence with the results (Gardner, L. (2005)), which is assumed to be caused by the waves across the width of the section. It may indicate that the buckling behaviour of EHS is more closely to plate behaviour rather than shell behaviour.

3.1.5 Further results and discussion

From the previous analysis, it can be seen that the difference of elastic buckling stress between ABAQUS results and Equation 2 results is mainly determined by aspect ratio and slenderness of an EHS. For further investigation on elastic buckling behaviour, EHS models with a wider range of aspect ratio as well as

smaller slenderness were set up and simulated using ABAQUS. Four different thickness values were chosen from 1 mm to 20 mm, while various degrees of aspect ratio ($D_1:D_2$) were attempted from 1:1 to 10:1, by means of keeping D_1 constant as 400 mm and changing D_2 values. The difference of elastic buckling stress between ABAQUS results and predicted equation results for each model is plotted in Figure 9 and shown in Table 3. The difference value is plotted against aspect ratio $D_1:D_2$ and four curvatures indicate four different slenderness of each model. Positive values indicate ABAQUS results are higher than equation 2 prediction.

D_1/D_2	Difference between ABAQUS results and Equation results			
	$t = 1$ mm	$t = 5$ mm	$t = 10$ mm	$t = 20$ mm
1.00	-0.90%	-0.90%	0.10%	0.12%
1.01	-0.02%	0.60%	0.20%	0.25%
1.05	0.21%	1.32%	0.80%	0.80%
1.10	0.38%	1.94%	2.83%	3.31%
1.25	1.61%	3.50%	5.07%	6.35%
1.50	2.10%	4.97%	7.00%	8.90%
1.75	2.60%	6.30%	8.50%	10.12%
2.00	3.07%	7.35%	10.69%	11.94%
2.25	3.62%	8.10%	11.60%	13.25%
2.50	3.89%	8.90%	12.50%	14.58%
2.75	4.09%	9.40%	13.50%	15.86%
3.00	4.31%	10.12%	14.29%	16.55%
3.50	4.73%	10.70%	14.90%	17.37%
4.00	5.06%	11.70%	15.90%	18.75%
5.00	5.82%	13.12%	17.35%	19.66%
7.50	6.75%	14.60%	19.80%	22.95%
10.00	7.63%	15.20%	21.74%	25.08%

Table 3. Differences of Elastic Buckling Stress between ABAQUS Results and Equation Results
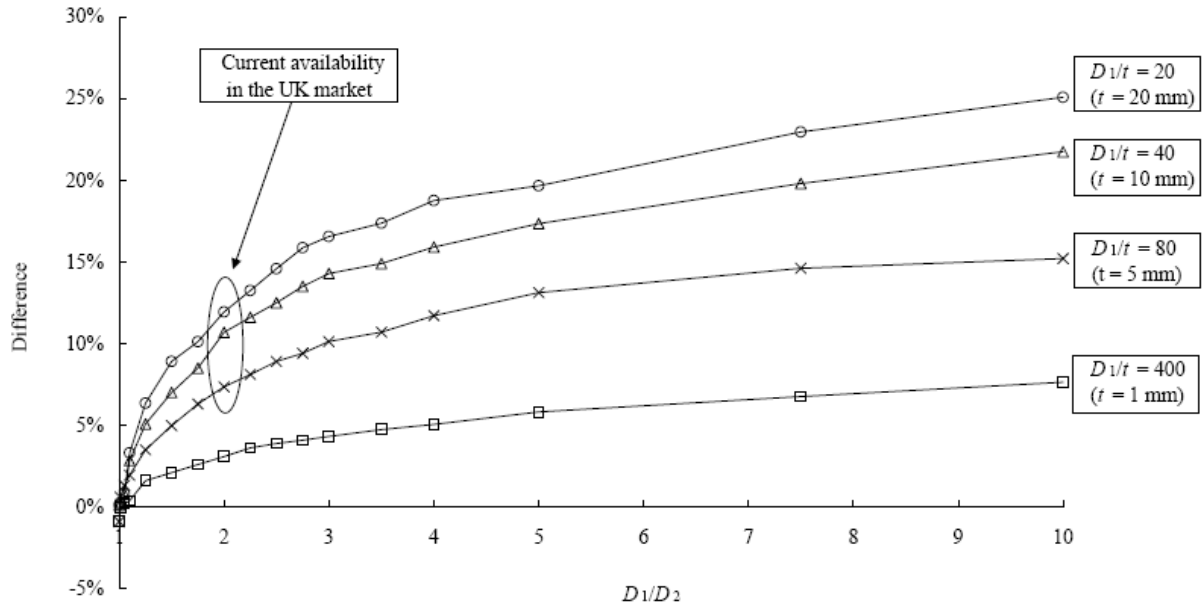
Figure 9. Differences of Elastic Buckling Stress between ABAQUS Results and Equation Results

From the results, it can be repeatedly observed that the discrepancy of elastic buckling stress between ABAQUS results and Equation prediction is affected by the aspect ratio and the slenderness of an EHS. With the increase of the eccentricity of an elliptical section (from circular shape to very flat shape), more significant difference is created. Moreover, the discrepancy is far greater for the compact models, compared to the slender ones.

The influence of aspect ratio (D_1/D_2) on this phenomenon is reasonably consistent with some previous researches. It was found in the early studies of elliptical shells (Kempner, J., Hutchinson, J.W., 1960s) that both theoretical and experimental initial buckling stresses for finite clamped cylinders with large out-of-roundness (severe eccentricity) are significantly greater than the classical buckling stresses obtained for a corresponding infinite shell. The reason may be the transition of the buckling behaviour of the EHS, from cylindrical shapes to very flat shapes, in which cases the classical equation may not accurately applied. Although the critical transitional behaviour was not clearly observed in the analyses, it is convinced that for those EHS having very large aspect ratios, their buckling behaviour is affected by the factors apart from cylindrical shell buckling, such as plate buckling. However, the inaccuracy for the severely eccentric elliptical sections are only of academic interest since the current availability of the EHS products are only having the aspect ratio as $D_1/D_2 = 2$.

Another influence of slenderness (D_1/t) on the discrepancy shows the limitations of the classical equation to predict the elastic buckling stress for varieties of EHS. This theoretical equation was derived in the assumption that the elliptical shells are slender enough, which would not entirely involve those EHS with

relatively low D_1/t ratio. A compact cross section with slenderness of 20 can not actually be treated as a shell which requires high slenderness of element. Nevertheless, it is not so important because it is at the extreme range of the specimens considered. The current available EHS designations are indicated in Figure 9, showing the ABAQUS results are approximately 10% higher than the prediction of Equation 2, which is not quite significant. It is conservative to apply the classical equation to calculate the elastic buckling stresses for various sorts of EHS; however, currently the equation still provides a relatively safe guide and method to estimate the elastic buckling stresses.

3.2 Elastic buckling with geometric imperfection

This stage investigated the behaviour of an EHS column and that of an equivalent CHS, assuming their material properties are elastic with some geometric imperfection as well. Some models of CHS were established in a similar way of EHS.

3.2.1 FEA model

Dimension of D_1:D_2 = 2.00, D_1 = 400 mm was selected as typical sectional properties. According to $D = D_1^2 / D_2$ which is the predicted equation to relate an EHS to an equivalent CHS concluded in Section 2, CHS with D = 800 mm was expected to behave similarly to an EHS (D_1:D_2 = 2.00, D_1 = 400 mm). Hence CHS models of this cross-section dimension were set up in the same way of EHS except the lengths of CHS were extended to 2400 mm to adapt the same L/D_1 ratio so as to guarantee the occurrence of local buckling. Furthermore, each group had three models of different thickness including t = 1 mm, 5 mm and 10 mm (D_1/t = 400, 80 and 40).

3.2.2 Analysis method

Finite element analyses were carried out both on EHS models and CHS models based on the method discussed in Section 2.4. Three different imperfections prescribed as percentages of the thickness which were $t/10$, $t/50$ and $t/100$ were input to observe how geometric imperfection affected the buckling stress of EHS and CHS. Figure 10 presents the buckling shape of an EHS caused by geometric imperfection using eigenvalue buckling analysis.
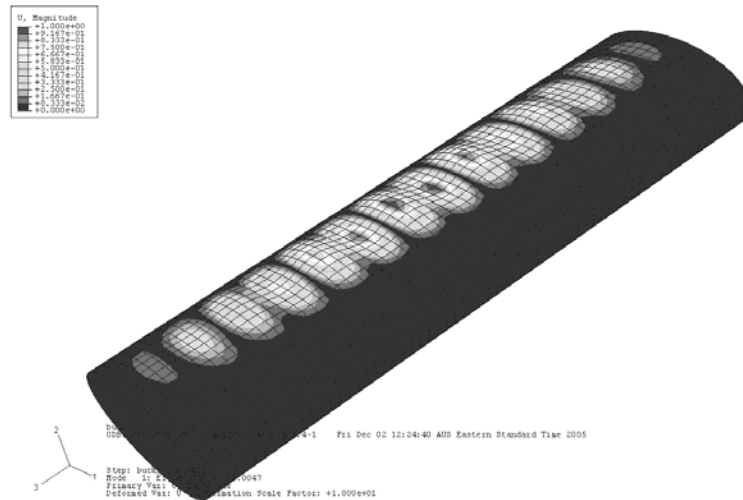
Figure 10. The Lowest Eigenmode of Buckling for EHS
(D_1:D_2 = 2.00, D_1/t = 80)

3.2.3 Results

Table 4 shows the results of the elastic buckling with geometric imperfection, where f_{crit} is the value of elastic buckling stress with no imperfection, and f_{ol} is the value of elastic buckling stress with certain imperfection. The value of f_{ol}/f_{crit} is calculated and shows the significance of imperfections on elastic buckling stresses.

EHS (D_1 = 400 mm = 2.00D_2), t = 10 mm, f_{crit} = 3445 MPa			CHS (D = 800 mm), t = 10 mm, f_{crit} = 3286 MPa		
Imperfection	f_{ol} (MPa)	f_{ol}/f_{crit}	Imperfection	f_{ol} (MPa)	f_{ol}/f_{crit}
$t/100$	3139	91.1%	$t/100$	2714	82.6%
$t/50$	2966	86.1%	$t/50$	2672	81.3%
$t/10$	2283	66.3%	$t/10$	1953	59.4%
EHS (D_1 = 400 mm = 2.00D_2), t = 5 mm, f_{crit} = 1668 MPa			CHS (D = 800 mm), t = 5 mm, f_{crit} = 1667 MPa		
Imperfection	f_{ol} (MPa)	f_{ol}/f_{crit}	Imperfection	f_{ol} (MPa)	f_{ol}/f_{crit}
$t/100$	1557	93.3%	$t/100$	1390	83.4%
$t/50$	1469	88.1%	$t/50$	1316	78.9%
$t/10$	1113	66.7%	$t/10$	1026	61.5%
EHS (D_1 = 400 mm = 2.00D_2), t = 1 mm, f_{crit} = 325 MPa			CHS (D = 800 mm), t = 1 mm, f_{crit} = 375 MPa		
Imperfection	f_{ol} (MPa)	f_{ol}/f_{crit}	Imperfection	f_{ol} (MPa)	f_{ol}/f_{crit}
$t/100$	300	92.3%	$t/100$	329	87.7%
$t/50$	285	87.7%	$t/50$	286	76.3%
$t/10$	222	68.3%	$t/10$	248	66.1%

Table 4. ABAQUS Results of Comparison of Elastic Buckling
with Geometric Imperfections

3.2.4 Discussion

From the results, it is observed that for all the models, larger imperfection induces lower buckling stresses. Table 4 shows how the elastic buckling load is reduced from the perfect specimen to a specimen with initial geometric imperfections. For sections with the same aspect ratio, the reduction in buckling stress f_{ol} is similar for the same relative imperfection size (eg. $t/100$) regardless of the slenderness of the section.

In addition, the reduction in buckling stress is greater for a CHS compared to the equivalent EHS. This means that the elastic local buckling stress of CHS is more sensitive to imperfections than the corresponding EHS. The results show reasonable agreement with early researches (Kempner, J., Hutchinson, J.W., 1960s) which indicated that an elliptical cylinder with sufficient eccentricity may be relatively insensitive to imperfections compared to a circular one. Hence, this illustrates that the behaviour of the equivalent CHS based on the equation $D = D_1^2/D_2$ does not exactly match that of the EHS. However, they behave similarly since the differences are averagely within 10%. To this extend, the approach to relate an EHS to a CHS is proved appropriate in the stage of elastic buckling with imperfections.

3.3 Inelastic buckling

The material properties of real structural products are non-linear with significant yielding stresses. This section investigates the effect of using close to real material properties in the analysis.

3.3.1 FEA model

A series of EHS models were set up with a range of aspect ratios from 1.25:1 to 3:1 followed by a series of the equivalent CHS models with a range of diameter from 500 mm to 1200 mm. Plastic material properties were added to all the models and the data input is shown in Table 5.

| Stress (MPa)	Strain
400	0.00
400	0.03
460	0.05
500	0.08
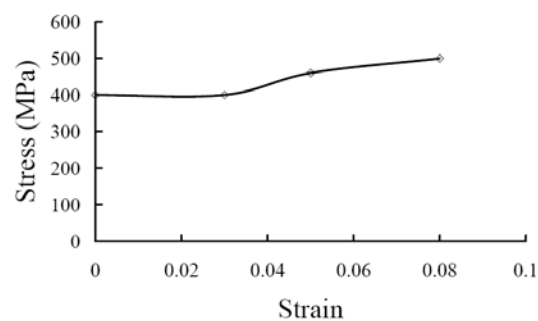
Table 5. Plastic Data Using in FEA Models

3.3.2 Analysis method

Generally, analysis were conducted on all the models of EHS and the equivalent CHS with the range of thickness changing from 30 mm to 1 mm and it is summarised that different D_1/t ratio changes the buckling behaviour of both EHS and CHS. Figure 11 shows the P/A_gf_y-Displacement diagram of an EHS

(D_1:D_2 = 2.00, D_1 = 400 mm), where P is the compressive load, A_g is the gross area of the cross section and F_y is the yield stress of the structural material.
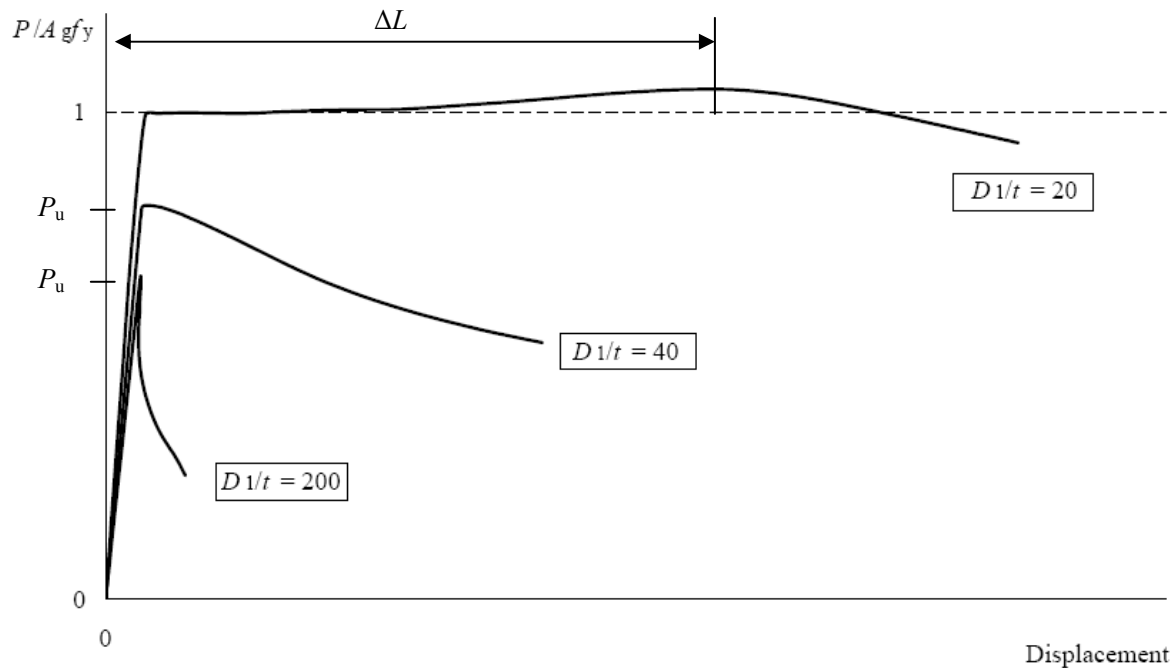
Figure 11. ABAQUS $P/A_g f_y$ -Displacement Curves of EHS
with Different D_1/t ratio

From this typical example, it is clearly observed that the compact ones reach yield stress prior to buckle, while the slender ones buckle before reaching yield stress.

For compact sections, there are little differences between the buckling stresses of EHS and that of the related CHS, since both sections fully reach the yield stresses. To verify the similarity of their behaviour, comparison of the deformation capacity prior to buckling is introduced. Deformation capacity represents the deformation during the stage from yielding to buckling which reflects the structural ductility. Hence, such comparison was considered in the analyses.

For slender sections, it is obvious that comparison of buckling stresses is significant. Focusing on this comparison, the inelastic buckling behaviour of EHS and the equivalent CHS could be examined.

In particular, two parts of analysis methods were tried due to the different buckling behaviours of compact models and slender models. As illustrated in Figure 4, for compact sections, ΔL, which indicates the displacement at which an EHS or a CHS reaches ultimate load P_u, was examined. The ratio of $\Delta L/L$ gives the structural ductility of EHS and CHS models because it explains the deformation during the stage from yielding to buckling. However, for slender sections, since they buckle prior to yield, the ratio of $P/A_g f_y$ is less than 1 and it

The University of Sydney

shows the percentage of the inelastic buckling stress divided by the yield stress. These two ratios of both EHS and the equivalent CHS deserved to investigate in this section.

3.3.3 Results

Table 6 & 7 show the results of comparison of the $\Delta L/L$ ratios for compact EHS and the equivalent CHS and that of $P/A_\text{g}f_\text{y}$ ratios for slender ones, respectively.

EHS				CHS				Difference
D_1/D_2	t	D_1/t	$\Delta L/L$	D	t	D/t	$\Delta L/L$	
1.25	18	22	1.52%	500	18	28	1.42%	6.58%
1.50	18	22	1.41%	600	18	33	1.34%	4.96%
1.75	18	22	0.81%	700	18	39	0.76%	6.17%
2.00	20	20	1.30%	800	20	40	1.22%	6.15%
2.25	25	16	1.98%	900	25	36	1.88%	5.05%
2.50	25	16	1.93%	1000	25	40	1.87%	3.11%
2.75	25	16	1.89%	1100	25	44	1.77%	6.35%
3.00	25	16	1.56%	1200	25	48	1.44%	7.69%

Table 6. ABAQUS Results of Comparison of the Ratio of $\Delta L/L$ for Compact Models

EHS				CHS				Difference
D_1/D_2	t	D_1/t	$P_\text{u}/A_\text{g}f_\text{y}$	D	t	D/t	$P_\text{u}/A_\text{g}f_\text{y}$	
1.25	0.8	500	0.892	500	0.8	625	0.887	0.56%
1.50	0.8	500	0.795	600	0.8	750	0.786	1.13%
1.75	1.0	400	0.851	700	1.0	700	0.831	2.35%
2.00	1.0	400	0.750	800	1.0	800	0.730	2.67%
2.25	1.0	400	0.666	900	1.0	900	0.676	1.50%
2.50	1.2	333	0.722	1000	1.2	833	0.725	0.42%
2.75	1.2	333	0.656	1100	1.2	917	0.671	2.29%
3.00	1.5	267	0.758	1200	1.5	800	0.755	0.40%

Table 7. ABAQUS Results of Comparison of the Ratio of $P/A_\text{g}f_\text{y}$ for Slender Models

3.3.4 Discussion

The results above show the difference of the $\Delta L/L$ ratios for the thick models are within 7%, and that of the $P/A_\text{g}F_\text{y}$ ratios for thin ones are within 3%, on average.

Hence, for slender sections which buckle elastically, the equivalent CHS gives a buckling stress very close to the EHS (within 3%). For compact sections, which exhibit a plastic plateau prior to yielding, the strains at buckling (or deformation capacity) for an EHS and the equivalent CHS are very similar (within 7%).

All EHS show slightly higher ductility than the equivalent CHS. Nevertheless, these results indicate that the equation $D = D_1^2/D_2$ provides reasonable agreement for the inelastic local buckling behaviours of EHS and CHS. This approach would be slightly conservative but safer to be applied due to the higher ductility in EHS models.

Gardner, L. (2005) noted that for a real EHS, the deformation at ultimate load is not reliably predicted using the FEA models because it is very sensitive to the exact level of imperfection. Since no imperfections were included for the models in the previous analysis, the results discussed can convincingly predict real models. However, for those models with geometric imperfections, the comparison of $\Delta L/L$ may vary. It is suggested this matter receive further attention in the further studies.

3.4 Simulation of real tests

Researchers at The University of Toronto (2005) performed some column tests of steel elliptical hollow sections under compression. Deformed shapes are shown in Figure 12. In this stage, ABAQUS was used to simulate the local buckling behaviour of the specimens of the real tests.

Figure 12. Deformed Shape of Specimen from Tests

3.4.1 FEA model

The section dimensions and material properties of the test specimen were shown in Table 8.

Dimensions			
Height (mm)	Width (mm)	Thickness (mm)	Area (mm^2)
221.2	110.9	5.94	3054

Tube material properties				
Coupon	E (MPa)	f_y (MPa)	f_u (MPa)	ε (%)
1	231	420.6	527.4	34.55
2	209	431.5	537.8	33.96
3	211	420.9	529.0	34.84
4	211	412.5	526.5	35.43
Average	215	421.4	530.2	34.70

Table 8. Cross-section Dimensions and Material Properties of the Specimens

The FEA model was established according to the actual section dimensions and material properties. The plastic data using in ABAQUS is shown in Table 9.

Stress (MPa)	Strain
420	0.000
422	0.015
424	0.018
428	0.029
439	0.034
462	0.045
479	0.056
500	0.078
511	0.097
516	0.108
520	0.123
525	0.133
529	0.175
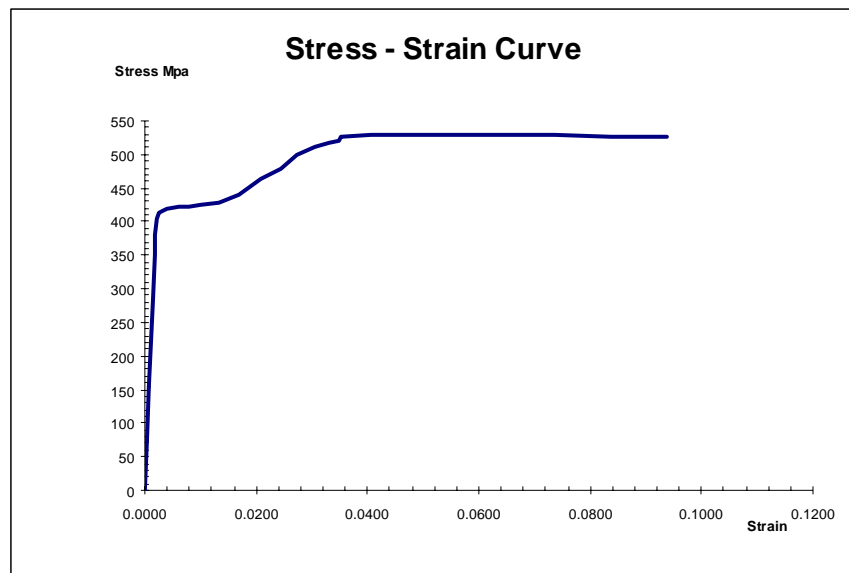
Table 9. Plastic Data of ABAQUS Models

3.4.2 Analysis method

Finite element analyses were carried out on the model of the real tests, in the method outlined in Section 2.4. Since the real tests did not include the measurement of real geometric imperfection of the specimen, different varieties of imperfection data were attempted in FEA and a couple of load-displacement curves were obtained respectively.

3.4.3 Results

The results of ultimate load P_u from tests as well as ABAQUS are shown in Table 10. Various geometric imperfections were applied. The differences between the ABAQUS results and the test results were obtained by the ratio of P_{ABAQUS}/P_{test}.

		P_u	P_{ABAQUS}/P_{test}
Real tests results		1392	
ABAQUS results with different imperfection	0	1314	94.40%
	$t/100$	1314	94.40%
	$t/50$	1312	94.25%
	$t/20$	1302	93.53%
	$t/10$	1286	92.39%

Table 10. Results from Real Tests and ABAQUS

Figure 13 plots the load-displacement curve obtained from the real specimen models as well as other three curves from the results of three different imperfection data which are $t/100$, $t/20$ and $t/10$ respectively. The buckling shapes of the models from ABAQUS are shown in Figure 14 & 15.
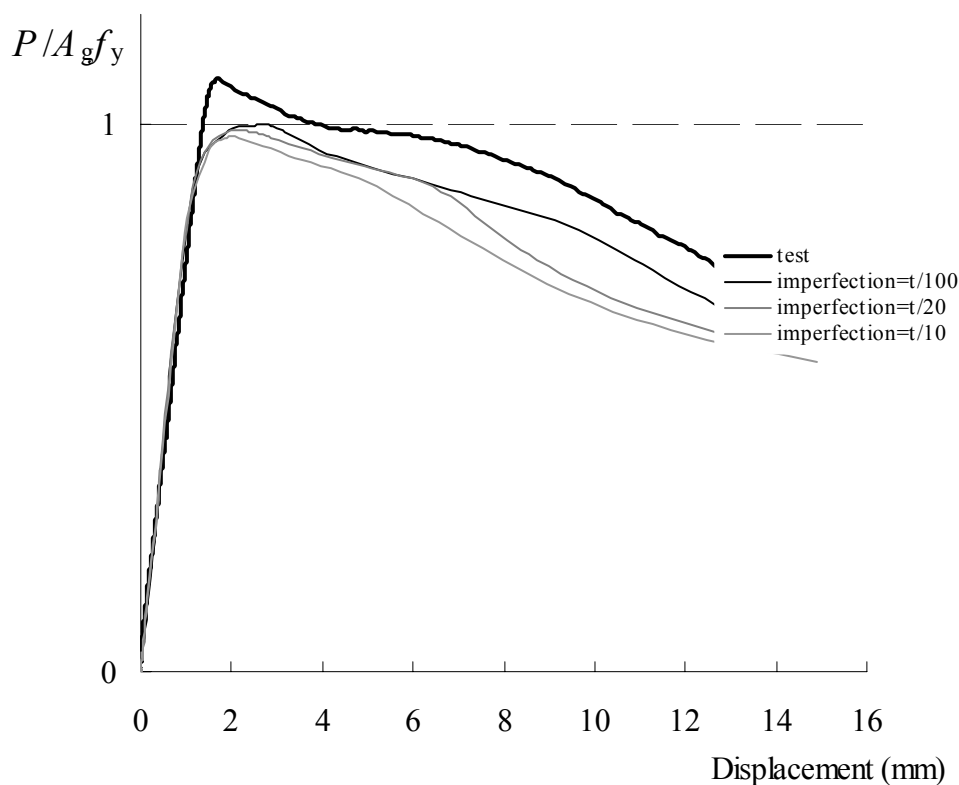
Figure 13. ABAQUS Load-Displacement Curves of Test Models
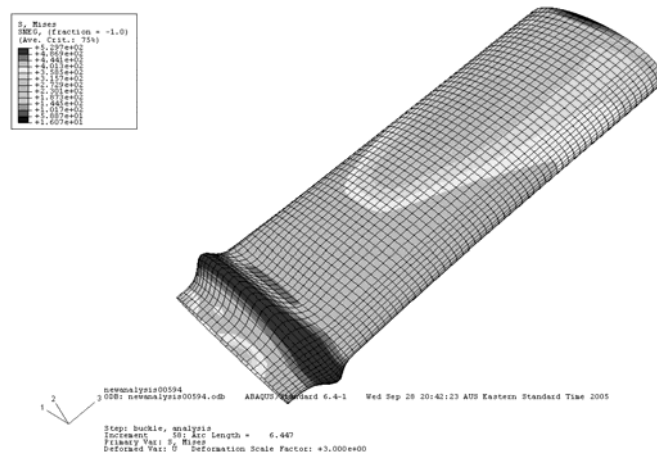
Figure 14. ABAQUS Local Deformed Shape of Test Model with
Imperfection = *t*/100
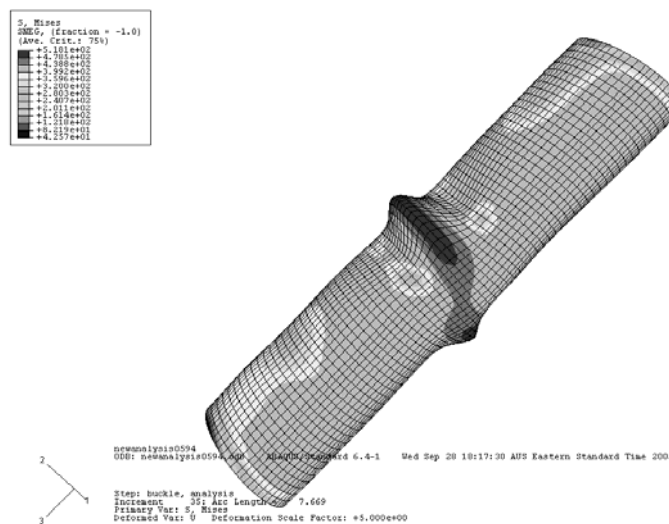
Figure 15. ABAQUS Local Deformed Shape of Test Model with
Imperfection = *t*/20

3.4.4 Discussion

Firstly, the FEA simulations tend to underestimate the experimental results. Even with zero imperfection, there is an underestimate of just over 5%. Possible reasons for this may include a slight discrepancy in the cross-section area when modeling a hollow section with a shell element. Also it is largely due to inaccurate material modeling, including use of tensile coupon tests to represent compressive stress-strain properties. In addition, the small yield stress spikes of the real specimen as shown in Figure 16 were not included in the FEA material properties.

Stress (MPa)
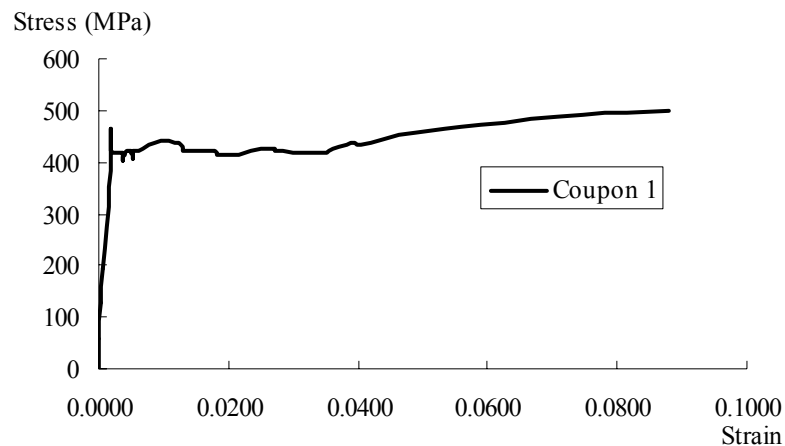
Figure 16. Strain – Stress Curve of Coupon 1 of Real Specimen

Since the experimental section were quite stocky ($D_1/t = 37$) and buckled after yielding, they are not so sensitive to geometric imperfections. Hence, it can be seen that the ABAQUS buckling load for various imperfection sizes (from $t/100$ to $t/10$) are very similar as yielding dominates the behaviour. The post buckling load shedding curves are similar in all cases.

For the buckling shapes, it can be seen that the deformed shape of the ABAQUS model with imperfection = $t/100$ (Figure 14) is quite similar to that of the experiments. However, since the test was performed singly at The University of Toronto, no more results could be referred for further detailed comparisons between numerical simulations and experimental tests.

4 Summary

This report has provided an introduction to the behaviour of structural steel elliptical hollow sections and described a series of finite element analysis on the columns of Elliptical Hollow Sections and the predicted equivalent Circular Hollow Sections using ABAQUS. Several stages of numerical simulations were conducted to get an overall understanding of local buckling behaviour of EHS and CHS.

The use of the finite element program ABAQUS for simulating the behaviour of the EHS and CHS columns was successful since the ABAQUS results were generally in good agreement with experimental values. The ABAQUS analyses gave reasonable and reliable results to be collected and compared with the calculation results of the predicted theory on EHS, through the stages of elastic, inelastic and real material properties.

Firstly, ABAQUS predictions of buckling stress of perfect EHS were approximately 10% higher than calculated results of equation $\sigma_{cr} = \dfrac{Et}{\left(\dfrac{A^2}{B}\right)\sqrt{3(1-v^2)}}$ (Marguerre, 1951 and Kempner, 1962). It was discussed that the results were consistent with early publications on the research. The discrepancy was also observed in the stage of elastic buckling with imperfections.

Secondly, the prediction of the equivalent CHS compared to an EHS using $D = D_1^2/D_2$ gave reasonably close approximation of buckling strain (ductility) once inelastic material properties were considered. This suggests that an equivalent CHS approach might be suitable in the section classification of EHS with regard to stub column strength, which has been recently attempted by Gardner, L. (2005). This approach would be slightly conservative but safer to be applied as higher ductility was observed in EHS models.

Thirdly, the ABAQUS analysis was compared to a single test results on a compact EHS. The FEA simulations were underestimating the experimental results due to several possible reasons.

Although a series of regular similarity were examined between EHS and CHS using the predicted equation, further comparison to a wider range of sections is required before this equivalent slenderness approach could be confirmed.

The University of Sydney

5 References

ABAQUS (2003). ABAQUS/ Standard User's Manual Volumes I-III and ABAQUS CAE Manual. Version 6.4. Hibbitt, Karlsson & Sorensen, Inc. Pawtucket, USA.

Gardner, L. (2005). "Structural behaviour of oval hollow sections", The Fourth International Conference on Advances in Steel Structures. June, 2005, Shanghai, China, pp. 517-522

Gardner, L. and Ministro, A. (2004). Testing and numerical modelling of structural steel oval hollow Sections. Department of Civil and Environmental Engineering Structures Section. Imperial college, UK.

Eckhardt, C. (2004). Classification of oval hollow sections. School of Civil Engineering Report. University of Southampton.

PrEN 10210-2, "Hot finished structural hollow sections of non-alloy and fine grain steels – Part 2: Tolerances, dimensions and sectional properties", CEN, 2003

Johnston, B.G. "Circular tubes and shells", Guide to stability design criteria for metal structures, third edition, pp 261-276, J.Wiley, New York, 1976.

Feinstein, G., Erickson, B. and Kempner, J. (1971). Stability of oval cylindrical shells. SESA Spring Meetings, Salt Lake City, Utah, May 1971.

Hutchinson, J. W. (1968). Buckling and initial post-buckling behaviour of oval cylindrical shells under axial compression. Transactions of the American Society of Mechanical Engineers, Journal of Applied Mechanics. March 1968, pp 66-72.

Kempner, J. (1962). Some results on buckling and post-buckling of cylindrical shells. Collected papers on Instability of Shell Structures. NASA TN D-1510, pp. 173-186.

The University of Toronto (2005), Unpublished test results of elliptical hollow section (EHS) stub columns in pure compression.

Riks E., "An incremental approach to the solution of snapping and buckling problems", Int. J. Solids Structures, Vol. 15, 529-551, 1979.

SCI (2003). Gross section properties of elliptical hollow sections. The Steel Construction Institute, UK.

6 Notation

A	major radii of an ellipse
A_g	gross area of cross section
B	minor radii of an ellipse
D	diameter
D_1	major diameter of an ellipse
D_2	minor diameter of an ellipse
E	Young's modulus of elasticity
f_{crit}	elastic buckling stress with no imperfection
f_{ol}	elastic buckling stress with certain imperfection
f_y	yield stress
l	length of a column
P	compressive load
P_{ABAQUS}	ultimate load from ABAQUS results
P_{test}	ultimate load from test results
P_u	ultimate load
σ_{cr}	elastic buckling stress
λ	eigenvalue from ABAQUS results
v	Poisson's ratio

7 Appendix

7.1 Tables of elastic buckling stress from ABAQUS results and predicted equation results

$D_1/D_2 = 1.00$				
Section Properties		Buckling Stress from ABAQUS (GPa)	Buckling Stress from Equation 2 (GPa)	Difference
D (mm)	t (mm)			
400	20.00	10.88	12.10	10.12%
400	16.00	8.76	9.68	9.48%
400	13.33	7.47	8.07	7.38%
400	11.43	6.59	6.91	4.70%
400	10.00	5.92	6.05	2.17%
400	8.89	5.37	5.38	0.23%
400	8.00	4.84	4.84	0.03%
400	7.27	4.41	4.40	-0.14%
400	6.67	4.05	4.03	-0.36%
400	6.15	3.74	3.72	-0.40%
400	5.71	3.47	3.46	-0.51%
400	5.33	3.25	3.23	-0.60%
400	5.00	3.05	3.03	-0.81%
400	4.71	2.87	2.85	-0.93%
400	4.44	2.78	2.69	-3.28%
400	4.21	2.57	2.55	-1.03%
400	4.00	2.45	2.42	-1.07%
400	3.81	2.33	2.30	-1.13%
400	3.64	2.23	2.20	-1.31%
400	3.48	2.13	2.10	-1.31%
400	3.33	2.04	2.02	-1.17%

Table 11. Elastic buckling stress from ABAQUS results and equation 2 results for model $D_1/D_2 = 1.00$

$D_1/D_2 = 1.25$					
Section Properties			Buckling Stress from ABAQUS (GPa)	Buckling Stress from Equation 2 (GPa)	Difference
D_1 (mm)	D_2 (mm)	t (mm)			
400	320	20.00	10.13	9.33	8.57%
400	320	16.00	8.14	7.52	8.27%
400	320	13.33	6.79	6.30	7.75%
400	320	11.43	5.82	5.42	7.43%
400	320	10.00	5.09	4.75	7.13%
400	320	8.89	4.53	4.23	6.91%
400	320	8.00	4.07	3.82	6.69%
400	320	7.27	3.70	3.47	6.49%
400	320	6.67	3.39	3.19	6.44%
400	320	6.15	3.13	2.95	6.18%
400	320	5.71	2.90	2.74	6.08%
400	320	5.33	2.71	2.56	5.98%
400	320	5.00	2.54	2.40	5.98%
400	320	4.71	2.39	2.26	5.99%
400	320	4.44	2.26	2.13	5.74%
400	320	4.21	2.14	2.02	5.77%
400	320	4.00	2.03	1.92	5.74%
400	320	3.81	1.94	1.83	5.70%
400	320	3.64	1.85	1.75	5.76%
400	320	3.48	1.77	1.67	5.68%
400	320	3.33	1.69	1.60	5.48%

Table 12. Elastic buckling stress from ABAQUS results and equation 2 results
for model $D_1/D_2 = 1.25$

$D_1/D_2 = 1.50$					
Section Properties			Buckling Stress from ABAQUS (GPa)	Buckling Stress from Equation 2 (GPa)	Difference
D_1 (mm)	D_2 (mm)	t (mm)			
400	267	20.00	8.87	7.88	11.22%
400	267	16.00	7.10	6.33	10.78%
400	267	13.33	5.89	5.30	10.00%
400	267	11.43	5.03	4.55	9.48%
400	267	10.00	4.39	3.99	9.04%
400	267	8.89	3.89	3.55	8.68%
400	267	8.00	3.49	3.20	8.36%
400	267	7.27	3.17	2.91	8.07%
400	267	6.67	2.90	2.67	7.91%
400	267	6.15	2.67	2.47	7.61%
400	267	5.71	2.48	2.29	7.41%
400	267	5.33	2.31	2.14	7.28%
400	267	5.00	2.16	2.01	7.20%
400	267	4.71	2.04	1.89	7.17%
400	267	4.44	1.92	1.79	6.88%
400	267	4.21	1.82	1.69	6.87%
400	267	4.00	1.73	1.61	6.80%
400	267	3.81	1.64	1.53	6.73%
400	267	3.64	1.57	1.46	6.75%
400	267	3.48	1.50	1.40	6.63%
400	267	3.33	1.43	1.34	6.44%

Table 13. Elastic buckling stress from ABAQUS results and equation 2 results for model $D_1/D_2 = 1.50$

$D_1/D_2 = 1.75$					
Section Properties			Buckling Stress from ABAQUS (GPa)	Buckling Stress from Equation 2 (GPa)	Difference
D_1 (mm)	D_2 (mm)	t (mm)			
400	229	20.00	7.87	6.82	13.29%
400	229	16.00	6.29	5.47	12.98%
400	229	13.33	5.21	4.57	12.21%
400	229	11.43	4.43	3.92	11.45%
400	229	10.00	3.86	3.44	10.88%
400	229	8.89	3.41	3.06	10.41%
400	229	8.00	3.06	2.75	10.01%
400	229	7.27	2.77	2.50	9.64%
400	229	6.67	2.53	2.30	9.42%
400	229	6.15	2.33	2.12	9.05%
400	229	5.71	2.16	1.97	8.80%
400	229	5.33	2.01	1.84	8.62%
400	229	5.00	1.88	1.72	8.49%
400	229	4.71	1.77	1.62	8.41%
400	229	4.44	1.67	1.53	8.10%
400	229	4.21	1.58	1.45	8.05%
400	229	4.00	1.50	1.38	7.95%
400	229	3.81	1.43	1.31	7.85%
400	229	3.64	1.36	1.25	7.84%
400	229	3.48	1.30	1.20	7.71%
400	229	3.33	1.24	1.15	7.49%

Table 14. Elastic buckling stress from ABAQUS results and equation 2 results for model $D_1/D_2 = 1.75$

$D_1/D_2 = 2.00$					
Section Properties			Buckling Stress from ABAQUS (GPa)	Buckling Stress from Equation 2 (GPa)	Difference
D_1 (mm)	D_2 (mm)	t (mm)			
400	200	20.00	7.05	6.04	14.33%
400	200	16.00	5.65	4.83	14.37%
400	200	13.33	4.68	4.03	13.83%
400	200	11.43	3.97	3.46	12.96%
400	200	10.00	3.45	3.02	12.21%
400	200	8.89	3.04	2.69	11.67%
400	200	8.00	2.72	2.42	11.17%
400	200	7.27	2.46	2.20	10.73%
400	200	6.67	2.25	2.02	10.43%
400	200	6.15	2.07	1.86	10.01%
400	200	5.71	1.91	1.73	9.71%
400	200	5.33	1.78	1.61	9.48%
400	200	5.00	1.67	1.51	9.31%
400	200	4.71	1.57	1.42	9.21%
400	200	4.44	1.48	1.34	8.85%
400	200	4.21	1.40	1.27	8.77%
400	200	4.00	1.32	1.21	8.65%
400	200	3.81	1.26	1.15	8.52%
400	200	3.64	1.20	1.10	8.49%
400	200	3.48	1.15	1.05	8.33%
400	200	3.33	1.10	1.01	8.08%

Table 15. Elastic buckling stress from ABAQUS results and equation 2 results for model $D_1/D_2 = 2.00$

$D_1/D_2 = 2.25$					
Section Properties			Buckling Stress from ABAQUS (GPa)	Buckling Stress from Equation 2 (GPa)	Difference
D_1 (mm)	D_2 (mm)	t (mm)			
400	178	20.00	6.31	5.43	13.94%
400	178	16.00	5.09	4.34	14.82%
400	178	13.33	4.23	3.61	14.57%
400	178	11.43	3.60	3.09	14.06%
400	178	10.00	3.11	2.70	13.07%
400	178	8.89	2.74	2.40	12.39%
400	178	8.00	2.45	2.16	11.85%
400	178	7.27	2.22	1.96	11.36%
400	178	6.67	2.02	1.80	11.06%
400	178	6.15	1.86	1.66	10.60%
400	178	5.71	1.72	1.54	10.27%
400	178	5.33	1.60	1.44	9.98%
400	178	5.00	1.49	1.35	9.77%
400	178	4.71	1.40	1.27	9.63%
400	178	4.44	1.32	1.20	9.23%
400	178	4.21	1.25	1.14	9.13%
400	178	4.00	1.18	1.08	8.97%
400	178	3.81	1.13	1.03	8.82%
400	178	3.64	1.07	0.98	8.77%
400	178	3.48	1.03	0.94	8.58%
400	178	3.33	0.98	0.90	8.32%

Table 16. Elastic buckling stress from ABAQUS results and equation 2 results for model $D_1/D_2 = 2.25$

$D_1/D_2 = 2.50$					
Section Properties			Buckling Stress from ABAQUS (GPa)	Buckling Stress from Equation 2 (GPa)	Difference
D_1 (mm)	D_2 (mm)	t (mm)			
400	160	20.00	5.71	4.94	13.52%
400	160	16.00	4.64	3.94	15.04%
400	160	13.33	3.86	3.28	15.14%
400	160	11.43	3.29	2.80	14.81%
400	160	10.00	2.85	2.45	14.14%
400	160	8.89	2.51	2.17	13.29%
400	160	8.00	2.24	1.95	12.65%
400	160	7.27	2.02	1.78	12.11%
400	160	6.67	1.84	1.63	11.77%
400	160	6.15	1.69	1.50	11.29%
400	160	5.71	1.56	1.39	10.95%
400	160	5.33	1.45	1.30	10.64%
400	160	5.00	1.36	1.22	10.42%
400	160	4.71	1.28	1.15	10.23%
400	160	4.44	1.20	1.08	9.81%
400	160	4.21	1.13	1.02	9.69%
400	160	4.00	1.08	0.97	9.50%
400	160	3.81	1.02	0.93	9.34%
400	160	3.64	0.97	0.88	9.27%
400	160	3.48	0.93	0.85	9.06%
400	160	3.33	0.89	0.81	8.79%

Table 17. Elastic buckling stress from ABAQUS results and equation 2 results for model $D_1/D_2 = 2.50$

| $D_1/D_2 = 2.75$ | | | | | |
| Section Properties | | | Buckling Stress from ABAQUS (GPa) | Buckling Stress from Equation 2 (GPa) | Difference |
D_1 (mm)	D_2 (mm)	t (mm)			
400	145	20.00	5.26	4.54	13.59%
400	145	16.00	4.23	3.61	14.53%
400	145	13.33	3.54	3.00	15.26%
400	145	11.43	3.03	2.56	15.25%
400	145	10.00	2.63	2.24	14.85%
400	145	8.89	2.31	1.99	14.11%
400	145	8.00	2.06	1.79	13.34%
400	145	7.27	1.86	1.62	12.73%
400	145	6.67	1.69	1.48	12.34%
400	145	6.15	1.55	1.37	11.84%
400	145	5.71	1.44	1.27	11.47%
400	145	5.33	1.33	1.19	11.17%
400	145	5.00	1.25	1.11	10.92%
400	145	4.71	1.17	1.04	10.73%
400	145	4.44	1.10	0.99	10.30%
400	145	4.21	1.04	0.93	10.13%
400	145	4.00	0.98	0.89	9.93%
400	145	3.81	0.94	0.84	9.75%
400	145	3.64	0.89	0.81	9.65%
400	145	3.48	0.85	0.77	9.44%
400	145	3.33	0.81	0.74	9.15%

Table 18. Elastic buckling stress from ABAQUS results and equation 2 results for model $D_1/D_2 = 2.75$

$D_1/D_2 = 3.00$					
Section Properties			Buckling Stress from ABAQUS (GPa)	Buckling Stress from Equation 2 (GPa)	Difference
D_1 (mm)	D_2 (mm)	t (mm)			
400	133	20.00	4.90	4.21	14.08%
400	133	16.00	3.88	3.34	13.77%
400	133	13.33	3.26	2.77	15.08%
400	133	11.43	2.79	2.37	15.33%
400	133	10.00	2.43	2.06	15.16%
400	133	8.89	2.15	1.83	14.78%
400	133	8.00	1.91	1.64	13.98%
400	133	7.27	1.72	1.49	13.27%
400	133	6.67	1.57	1.37	12.82%
400	133	6.15	1.44	1.26	12.26%
400	133	5.71	1.33	1.17	11.88%
400	133	5.33	1.23	1.09	11.53%
400	133	5.00	1.15	1.02	11.28%
400	133	4.71	1.08	0.96	11.07%
400	133	4.44	1.01	0.91	10.60%
400	133	4.21	0.96	0.86	10.44%
400	133	4.00	0.91	0.81	10.20%
400	133	3.81	0.86	0.78	9.99%
400	133	3.64	0.82	0.74	9.89%
400	133	3.48	0.78	0.71	9.66%
400	133	3.33	0.75	0.68	9.34%

Table 19. Elastic buckling stress from ABAQUS results and equation 2 results for model $D_1/D_2 = 3.00$